05

Feature of infiltration under the action of capillary forces of the silicon melt to a great depth of porous carbon material

© V.A. Tyumentsev,[1] A.G. Fazlitdinova,[1] A.B. Liberzon[2]

[1]Chelyabinsk State University,
454001 Chelyabinsk, Russia
[2]SilKam,
454780 Ozersk, Chelyabinsk Region, Russia
e-mail: tyum@csu.ru

Received August 2, 2023
Revised November 28, 2023
Accepted December 25, 2023

The results of X-ray diffraction and electron microscopic studies of composite materials obtained in the process of directional impregnation from bottom to top of carbon bases differing in porosity at a temperature of $\geq 1500^{\circ}$C with a KR-00 grade silicon melt are considered. Results of *in situ* observation of the interaction of silicon melt with a porous carbon base. It is shown that an increase in the apparent density of the porous carbon matrix over 1.452 g/cm^3 limits the height of silicon melt infiltration; In the transition region, only SiC phases and graphite are present; the silicon melt that enters this region completely enters into solid-phase interaction with carbon. The surface of the largest pores turned out to be covered with a layer of silicon carbide.

Keywords: carbon-silicon carbide composite, reactive infiltration, X-ray diffraction analysis, phase composition.

DOI: 10.21883/0000000000

Introduction

C-SiC composite materials have unique properties such as high chemical and abrasive resistance, low coefficient of thermal expansion, relatively high thermal conductivity, radiation stability, low friction coefficient, and are widely used in areas of techno-progress [1–7], in particular, in the petrochemical industry, shipbuilding and fuel and energy enterprises. An effective process for producing C-SiC composite materials is the reactive infiltration of molten silicon into a porous carbon material. The melt impregnates the porous carbon workpiece under the action of capillary forces and interacts with the carbon. The process of infiltration of molten Si into porous carbon is usually considered to consist of rapid non-reactive infiltration and subsequent interaction of silicon and carbon with the formation of a thin ($\sim 10\,\mu$m) dispersed layer of SiC at the interface. Then, with subsequent isothermal holding of the material, along with the continuation of the interaction of the melt with carbon, recrystallization of dispersed SiC and the formation of larger faceted crystals develops [5,7]. In this case, it is assumed that the infiltration rate is controlled by the viscous resistance of the melt. As a result, a composite material is formed, the content of SiC in which (depending on the pore structure of the workpiece and synthesis conditions) can range from ~ 35 to ~ 70 mass.%, and metallic silicon from 5 to 15 mass.%, the rest is polycrystalline graphite [6].

To better understand the mechanism of melt penetration into a porous carbon material, in a slew of works have studied, including the *in situ* method, the interaction of a drop of silicon melt with a carbon substrate. The dependence of the contact angle of wetting for a melt droplet on the time and temperature of heat treatment has been determined for various carbon materials [2.7–9]. It has been shown that as a result of the interaction of the Si melt with carbon, a thin layer of SiC is formed, which significantly reduces the contact angle of wetting. It is also noted that the interaction of the silicon melt with carbon proceeds faster than infiltration [10]. This gave reason to believe that the infiltration process is controlled by the formation of a thin layer of the reaction product as the melt moves through the pores. The process of carbon dissolution in silicon and the formation of a new SiC phase is accompanied by a significant endothermic effect [4,6,7,10,11]. As a result of the reaction between Si and carbon, the magnitude of the local temperature increase at the infiltration front through the porous carbon material can be tens and even hundreds of degrees [6,7]. A significant endothermic effect during the interaction of a melt with a porous carbon workpiece heated to $\sim 1500^{\circ}$ can promote the occurrence of a reaction of the type of self-propagating high-temperature synthesis [5]. It is also believed that the endothermic effect of the reaction between molten silicon and carbon complicates the infiltration process, reducing permeability due to the formation of SiC. The kinetics of infiltration is significantly affected by the melt temperature, morphology and pore size, and the nature of the carbon material [6,11–14]. However, the mechanism of reactive infiltration of the silicon melt, the sequence of the solid-state reaction and impregnation of the porous carbon base with the melt remain insufficiently studied. In [15], using

Table 1. Apparent density (ρ_0), porosity (Π_{tot}) of samples and the rise lifting of the silicon melting depending on the charge weight

Sample No	Change of weighed portion of charge weight, mass.%	ρ_0, g/cm^3 Porous carbon matrix	Π_{tot}, % Porous carbon matrix	Rise lifting melting	ρ_0, g/cm^3 after mm siliconizing
1	Initial charge weight	1.383	38.0	105	2.58
2	−10	1.245	44.2	105	2.5
3	−20	1.11	50.2	105	2.4
4	+10	1.52	31.8	30	–
5	+20	1.66	25.6	12	–
6	Initial charge weight	1.383	38.0	105	2.58
7	+2.5	1.42	36.3	105	–
8	+5	1.452	38.9	75	–
9	+10	1.52	31.8	32	–

a specially created high-temperature furnace, the infiltration of Si melt in slot-type capillaries was studied in detail. It has been shown that the capillary effect does not control the infiltration rate; an important component of the process is the interaction of silicon with carbon through the gas phase.

In this work, in order to clarify the mechanism of infiltration, the results of X-ray diffraction, electron microscopic and electron probe studies of composite materials obtained in the process of directed impregnation from below to a height of up to 105 mm of carbon bases, characterized by porosity, at a temperature of $\sim 1500^\circ$ with silicon melt Grade KR-00 are considered The results of *in situ* observation of the interaction of a silicon melt with a porous carbon base, a study of the phase composition and distribution of elements in the sample after interaction during period ~ 6 s are presented.

1. Objects and methods of study

A carbon porous base was obtained by pressing into a closed die a given amount of powder of graphitized material (Grade of graphite GMZ-0) with particle sizes from ~ 0.0 to 0.5 mm, mixed with a binder, i.e. phenol-formaldehyde resin in an amount of 15 mass.%. The pressed workpiece was polymerized and then carbonized in an inert environment at $\sim 800^\circ$C. The loss in the mass of carbon material after carbonization ~ 6.5 mass.%. The apparent density of the porous carbon base ρ_0, equal to the ratio of the weight to the volume of the sample, was set by changing the amount of press powder placed in a closed die, the final volume of which remained the same during pressing. Thus, two series of porous carbon substrates were obtained. The calculated apparent density ρ_0 and total porosity Π_{tot} of five carbon bases of the first series No 1−5and four of the second series No 6 − 9 are given in Table 1. The total porosity of the material was calculated using the formula: $\Pi_{tot} = (\rho - \rho_0)/\rho$ (true density value of graphitized material$\rho = 2.23$ g/cm^3 [11]).

To study the patterns of formation of a carbon-silicon carbide composite in the process of directed infiltration of carbon material with molten silicon, samples of size $20 \times 20 \times 105$ mm, were made, differing in the value of apparent density. It was planned to establish the relationship between the lifting rise of the silicon melt during infiltration and the pore structure of the carbon matrix, as well as the distribution of the phase and elemental compositions of the resulting composite material according the height of the siliconized samples. Carbon samples of the first series were vertically fixed in a special mechanism, which provided simultaneous supply from below of silicon melt of the Grade KR-00 (the content of Al, Fe and Ca impurities is no more than 0.3, 0.4 and 0.4%, respectively), located at a temperature of $\sim 1450^\circ$C. The mechanism, together with samples of carbon materials, was heated in a vacuum before impregnation with the melt $\sim 10^{-2}$ mm Hg to a temperature of $\sim 1600^\circ$C. Samples of siliconized materials of the second series were obtained in the same way. The duration of the samples' stay in the furnace at temperature $\sim 1600^\circ$C after contact with the melt was 30 min.

To study the porous structure of the carbon base and the C-SiC composite, as well as the spatial distribution of silicon and silicon carbide, the lateral surface of the samples obtained after silicification was polished with a diamond tool. X-ray phase analysis of the composite was carried out using a D8 ADVANCE diffractometer, Bruker (filtered CuKα— radiation) in the Bragg-Brentano geometry (scanning θ/θ, angularly step 0.05 °). The average sizes of coherent scattering regions (CSR) were calculated using the Selyakov-Scherrer formula: $L = k\lambda/\beta\cos\theta$, where constant $k = 1$, wavelength $\lambda = 1.5418$ Å, β — integral width of the diffraction maximum. Interplanar spacings were calculated from the center of gravity of the diffraction maxima. In the

process of X-ray diffraction studies, in order to average the results over a larger volume of the composite, the samples were rotated in the horizontal plane at a speed of 15 rpm. To study the distribution of the phase composition of the composite at the boundary of „impregnated and unimpregnated" part of the porous carbon workpiece with molten silicon, the width of a flat X-ray beam was minimized (the width of the slit aperture of the diffractometer was 0.2 mm). In this case, the sample was fixed and positioned so that the plane of the X-ray beam was parallel to the boundary between the impregnated and unimpregnated part of the composite. Initially, a phase analysis was carried out on the unimpregnated part of the carbon base, then the sample was successively shifted towards the impregnated part until weak maxima of other phases appeared. Next, the sample was shifted with a step of ~ 1 mm and X-ray patterns were recorded. The assessment of the porous structure and spatial homogeneity of the resulting composite material by elemental composition was carried out using a JSM 6510LA scanning-electron microscope equipped with an energy-dispersive spectrometer. To observe *in situ* the interaction of the silicon melt with carbon, a sample was prepared from a porous carbon base No 1 with dimensions $90 \times 6 \times 6$ mm. In the center, by a width of 30 mm, the thickness of the sample was reduced to 3 mm and pieces of silicon were placed on this area. Heating was carried out by passing a current through the sample at air pressure of 10^{-2} mm Hg.

2. Results and discussion

The silicon melt, located at a temperature of $\sim 1450^{\circ}$C, entered the lower bowl of the mechanism, in which samples with a height of 105 mm were installed, and, under the action of capillary forces, it were lifted up through the porous matrix, pre-heated to a higher ($\sim 1600^{\circ}$C) temperature. In the result of the simultaneously carried out silicon infiltration in five samples of the first series, it turned out that in porous carbon materials, the ρ_0 of which are ~ 1.383, ~ 1.345 and ~ 1.11 g/cm^3 (total porosity Π_{tot} respectively ~ 38, ~ 44, ~ 50 mass.%) the melt is raised up 105 mm. In samples, ρ_0 of which ~ 1.52 and ~ 1.66 g/cm^3, the melt is raised up through the pores to a height of ~ 30 and~ 12 mm. Only the lower part of the samples turned out to be siliconized. Samples No 6 and No 7 of the second series (ρ_0 carbon bases 1.383 and 1.42 g/cm ^{3}) also turned out to be impregnated with silicon to a height of 105 mm. In samples No 8 and No 9 (ρ_0 carbon bases, respectively, ~ 1.452 and ~ 1.52 g/cm^3), the silicon melt is raised up to a height of~ 75 and ~ 32 mm (Table 1).

On thin metallographic samples No 4 and 5, 8 and 9, partially impregnated with molten silicon, a transition area is observed at the boundary of the impregnated-unimpregnated part of the porous carbon workpiece. The width of such an area ranges from ~ 4 to ~ 6 mm. The change in the phase composition in the transition area of the sample No 8 with a sequential shift of the X-ray diffraction recording region towards the impregnated part is illustrated in Fig. 1 and Table 2. In the first X-ray diffraction pattern obtained from an unimpregnated section of a carbon workpiece, located ~ 10 mm away from the transition region, a characteristic and most intense maximum of 002 graphite is observed. In the X-ray diffraction patterns *2* and *3*, along with the maximum 002 of graphite, maxima β-SiC are revealed, the intensity of which gradually increases, the sample becomes two-phase. The characteristic and most intense maximum 111 of silicon in the X-ray diffraction pattern *4* appears after an additional displacement of the sample by ~ 2 mm. With a further shift of the phase composition recording region by ~ 5 mm, the intensity of the silicon maxima increases (this region is located at a

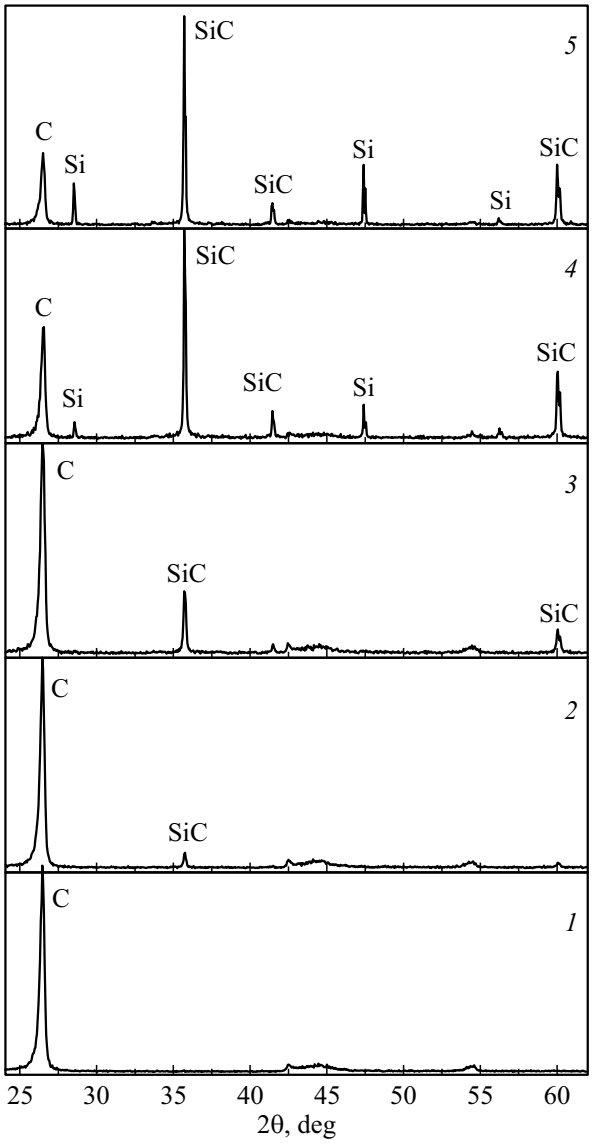

Figure 1. X-ray patterns of a carbon matrix not impregnated with a silicon melt (*1*), at the boundary the unimpregnated part — transition region (*2*, *3*), material of the transition region (*4*) and the composite beyond the transition region (*5*) (Table 2).

Table 2. Change in the phase composition of the composite with sequential displacement of the X-ray recording area at the impregnated-unimpregnated part boundary towards the sample area impregnated with the silicon melt No 8

No	Areas of X-ray recording at the boundary „impregnated and unimpregnated“ part	Phase composition, mass.%		Interplanar distance, Å	CSR dimensions, nm
1	Unimpregnated carbon matrix	C	100	$d_{002} = 3.381$	$L_{002} = 28$
2	Appearance of 111 SiC maximum at the boundary	C	94	$d_{002} = 3.385$	$L_{002} = 30$
		SiC	6	$d_{111} = 2.513$	$L_{111} = 52$
3	Area of X-ray recording is shifted to$\sim$ 1 mm	C	54	$d_{002} = 3.383$	$L_{002} = 33$
		SiC	46	$d_{111} = 2.514$	$L_{111} = 46$
4	Area of X-ray recording is additionally shifted to $\sim$ 2 mm	C	39	$d_{002} = 3.385$	$L_{002} = 29$
		SiC	57	$d_{111} = 2.514$	$L_{111} = 59$
		Si	4	$d_{111} = 3.125$	$L_{111} = 70$
5	Area of X-ray recording is additionally shifted to $\sim$ 5 mm	C	29	$d_{002} = 3.384$	$L_{002} = 33$
		SiC	58	$d_{111} = 2.514$	$L_{111} = 62$
		Si	13	$d_{111} = 3.131$	$L_{111} = 69$

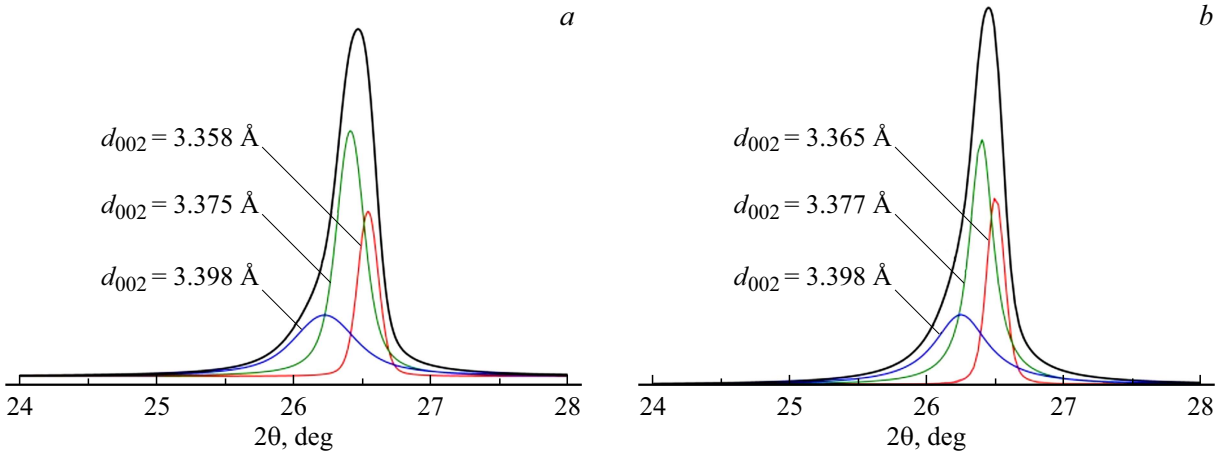

Figure 2. Profiles of asymmetric diffraction maxima of 002 graphite in the X-ray recording patterns *1* (*a*) and *5* (*b*), and the results of decomposition into three symmetric components.

height of $\sim$ 60 mm from the bottom cut of the sample). The ratio of the graphite/β-SiC/Si phases in the sample becomes approximately equal to 29/58/13 wt.%, respectively. The phase composition of the graphite/β-SiC/Si sample at a height of $\sim$ 10 mm differs slightly from the lower cut and amounts to $\sim$ 27/59/14 mass.%, respectively.

The diffraction maxima 002 of the carbon material in the recording regions of X-ray diffraction pattern 1−5 of the studied sample are asymmetric and can be presented as the sum of three symmetric maxima (Fig. 2). This, as shown in [16], can be due to the simultaneous presence of three components (metastable carbon states), differing in the value of the interplanar spacing d_{002}. From the calculation data given in Table 3, it follows that during the process of infiltration of the silicon melt and the formation of a new β-SiC phase, no significant changes in the structure of the carbon material are observed.

On thin metallographic samples of samples No 4, 5 and 9, characterized by a denser porous carbon base, the transition region at the boundary of the impregnated-unimpregnated part of the porous carbon workpiece is narrower $\sim$ 4 mm. The phase composition of the impregnated part of carbon blanks, differing in total porosity Π_{tot} at a height of $\sim$ 10 and $\sim$ 90 mm from the bottom cut of the samples, is given in Table 4. From the data in Tables 1 and 4 it follows that a decrease in the porosity of the carbon base significantly affects the height of the rise of the melt through the pores and the content of silicon carbide and unreacted carbon in the composite. It should also be noted that in the studied samples there is a tendency for the amount of silicon carbide

Table 3. Component composition of the carbon material of the composite with sequential displacement of the X-ray recording area at the boundary of the impregnated and unimpregnated part towards the sample area impregnated with the silicon melt No 8

No	Areas of X-ray diffraction pattern at the boundary impregnated and unimpregnated part	Interplanar spacing d_{002} component, Å	Dimensions of CSR L_{002} component, nm	Coefficient of determination R^2
1	Unimpregnated carbon matrix	3.358	52	0.9978
		3.375	38	
		3.398	17	
2	Appearance of 111 SiC maximum at the boundary	3.365	61	0.9941
		3.377	37	
		3.397	15	
3	Area of X-ray recording is shifted to$\sim$ 1 mm	3.361	53	0.9930
		3.376	47	
		3.391	18	
4	Area of X-ray recording is additionally shifted to $\sim$ 2 mm	3.364	53	0.9965
		3.379	36	
		3.393	13	
5	Area of X-ray recording is additionally shifted to $\sim$ 5 mm	3.365	61	0.9932
		3.377	42	
		3.398	18	

formed to decrease by 10−15 mass.% $\sim$ 90 mm at a height of $\sim$ 90 mm compared to the lower part. This may be due to the noticeably shorter interaction time of silicon with the porous carbon base due to the rather slow infiltration of the melt (the time of contact of the lower part of the carbon base with the silicon melt is 30 min).

When observing *in situ* the interaction of a silicon melt with carbon, initially the temperature of the thinnest part of the sample and silicon was brought to $\sim 900^\circ$C, then gradually increased to $\sim 1500^\circ$C during period 2 s. At this temperature, the thin part of the sample was kept for $\sim$ 2 s, after which a sharp increase in temperature was observed at $\sim 100 - 150^\circ$C (flare), which lasted less than 1 s. Then the temperature of this area visually decreased to the initial one ($\sim 1500^\circ$ C, the magnitude of the electric current through the sample was not changed). The sample was kept at this temperature for 3−4 s, after which the power supply was turned off. As a result, it turned out that the silicon melt penetrated through and through a 3/mm thick porous carbon plate located under the pieces of silicon. The diameter of such impregnated areas is $\sim$ 5 mm. The boundary of the impregnated and unimpregnated parts of the sample is visible quite clearly (Fig. 3, *a*), diffuse penetration of silicon into the porous carbon base is not observed by electron probe microanalysis. Using X-ray diffraction analysis, the β -SiC, Si and C phases are detected in the sample. Thus, the process of interaction between the Si and C melt is accompanied by a visually observable strong exo-effect. During $\sim$ 6 s solid-phase interaction, not all of the silicon melt entered into the reaction of forming silicon carbide.

Let us consider the results of electron microscopic studies of the pore structure and spatial distribution of the elemental composition in the studied samples. Fig. 3, *b* shows an electron microscopic image of a thin metallographic sample of the initial carbon matrix of sample No 1. The cross-sectional pore sizes range from $\sim$ 10 to $\sim 100\,\mu$m. The pore walls are not smooth, they are formed by the smallest fraction of the press powder, monolithized by carbon formed during the carbonization of the binder, i.e. phenol-formaldehyde resin. In thin metallographic sample of a composite material obtained by liquid-phase reactive infiltration (distance $\sim$ 10 mm from the bottom cut of the sample), there are no pores, more contrasting graphite particles, silicon carbide and silicon that have not interacted are observed (areas of lighter contrast in Fig. 3, *c*). The characteristic X-ray emission spectra of such regions contain only silicon and carbon lines. Weak spectral lines of impurities (Al, Fe and Ca, the total amount of $\sim$ 1.1 mass.%), which are present in the composition of the KR-00 silicon melt, were not detected.

In electron microscopic images of the composite in the transition area, the phase composition of which, according to X-ray diffraction analysis, is represented only by graphite and silicon carbide, the smallest and largest pores, completely and partially filled with the new phase, respectively,

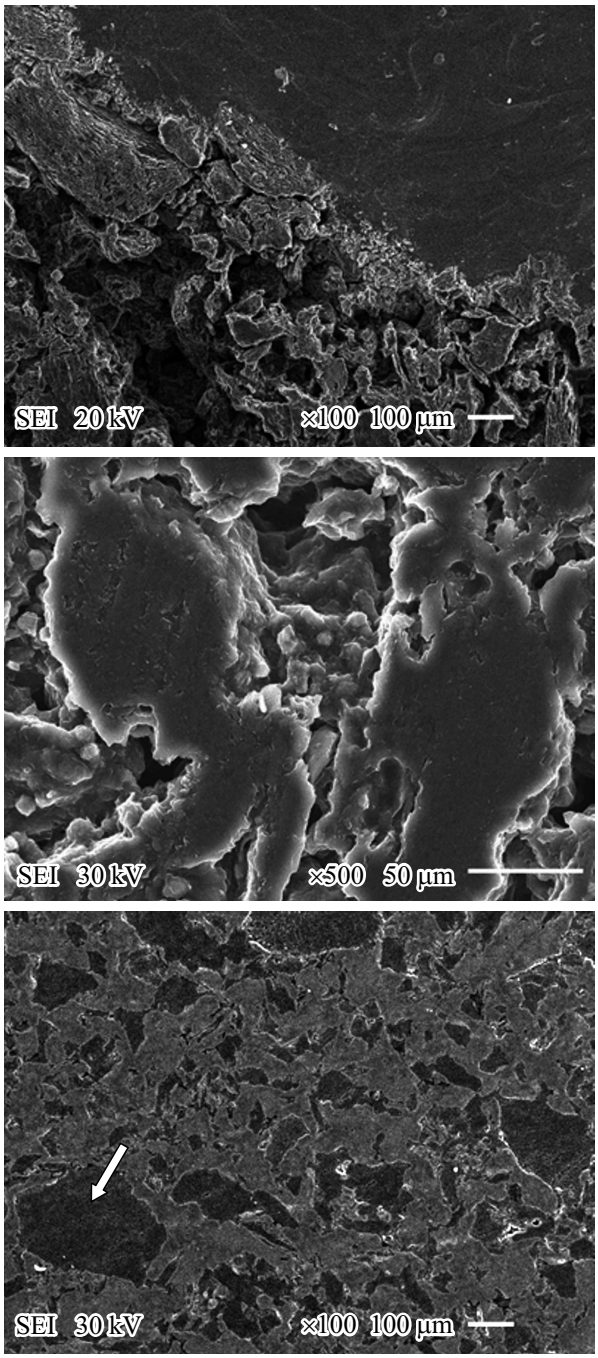

Figure 3. Electron microscopic image: *a* — boundaries of molten-impregnated silicon and porous carbon substrate; *b* — surface of the pore wall formed by the finest fraction of the press powder; *c* — metallographic samples (graphite particles are darker, marked with an arrow for example).

are observed (Fig. 4, *a*). The spectra of characteristic X-ray radiation obtained from the phase marked with the number *1* (the most contrasting areas in the electron microscopic image) contain carbon lines (Table 5). On the X-ray spectra obtained from the phase with a lighter contrast, marked with the number *2*, as a rule, only intense lines of silicon and carbon are observed. Silicon carbide

Table 4. Relationship between the total porosity (Π_{tot}) of the carbon matrix and the phase composition of the resulting composite material at a height of$\sim$ 10, $\sim$ 50 and $\sim$ 90 mm from the bottom cut of the sample.

Sample No	Porosity matrix Π_{tot}%	Distance upto regions of registration, mm	Phase composition composite, mass.%		
			SiC	C	Si
1	38.0	90	49	27	24
		50	53	28	19
		10	58	31	11
2	44.2	90	55	30	15
		50	53	29	18
		10	61	24	15
3	50.2	90	48	21	31
		50	51	17	32
		10	63	23	14
8	38.9	60	58	29	13
		10	59	27	14
4	31.8	10	52	39	9
5	25.6	10	53	41	6

covers the surface of large pores from the inside and inherits the surface topography. At some points of the phase covering the surface of the pores, small amounts of Al, Fe and Ca impurities can be detected (for example, in the figure at point 3, Table 5). However, there are micro-areas in which the content of some impurities significantly exceeds their amount in the original Grade KR-00 silicon. Fig. 4, *b* shows an electron microscopic image of a section of the composite in the light of secondary electrons and characteristic X-ray radiation of calcium, carbon and silicon (respectively *c*, *d*, *e*). At the points *4* and *5* marked in the figure, Ca is present, the amount of which exceeds 28 and 9 mass.% (Table 5).

Thus, silicon can, by surface diffusion (or by wetting the pore surface), move over a distance on the order of the width of the transition zone between the impregnated and unimpregnated regions of the carbon porous matrix. A noticeable difference between the formed silicon carbide in the lower and upper parts of the carbon porous workpiece may indicate that the process of infiltration of the silicon melt proceeds quite slowly. It can also be assumed that at the initial moment of contact of the silicon melt with the porous carbon matrix, the process of solid-phase interaction is accompanied by a significant endothermic effect. As a result, a layer of a new β-SiC. phase is formed. Liquid-phase infiltration of the melt follows the surface spreading

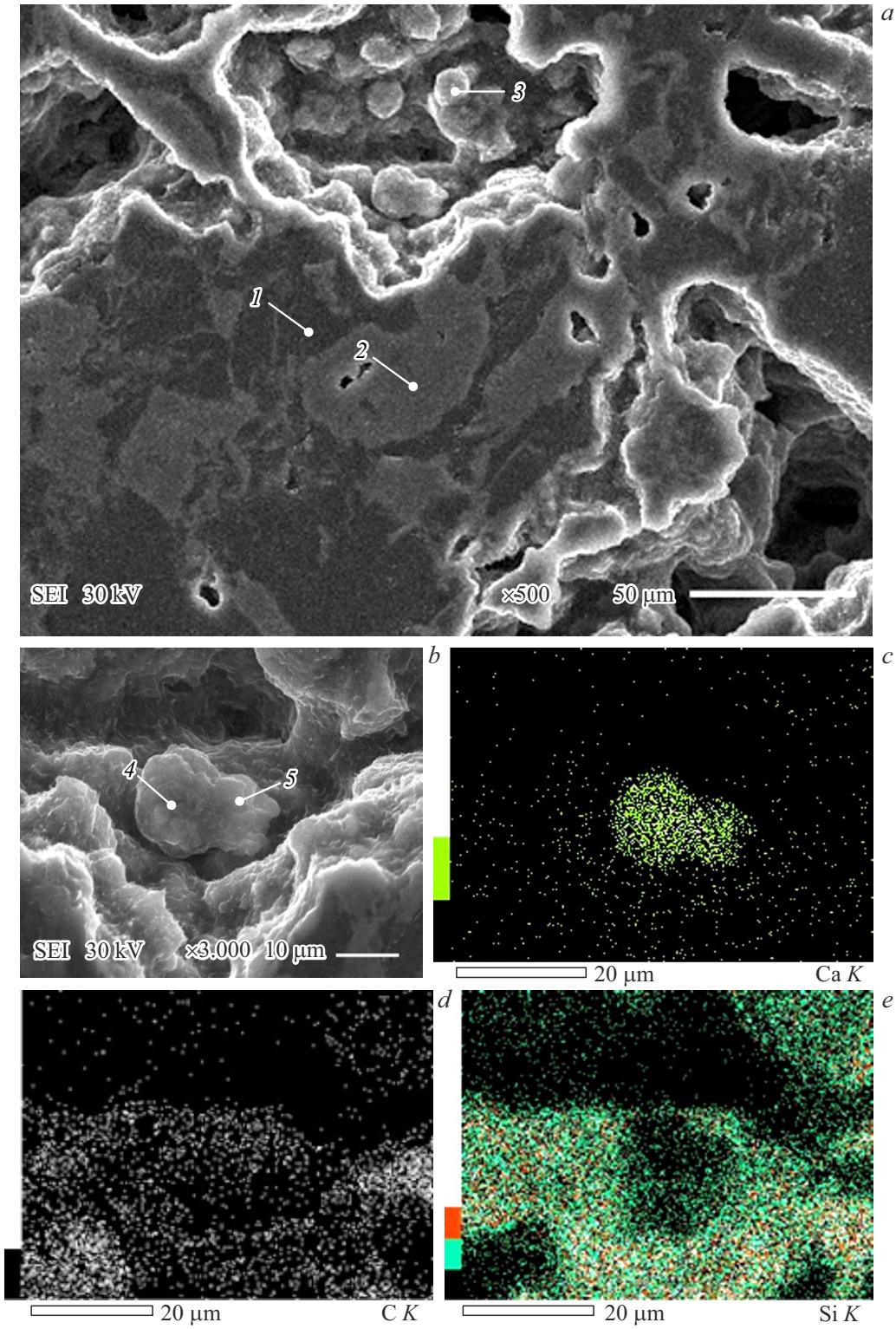

Figure 4. Electron microscopic image of the composite in the transition area (*a*, *b*), numbers 1–5 indicate the points of registration of the elemental composition of the material (Table 5); image fragment in the light of electrons (*b*) and characteristic X-ray radiation of calcium (*c*), carbon (*d*) and silicon (*e*).

of silicon. Since the rate of melt infiltration is low, the magnitude of local overheating of the transition region should not significantly affect the formation of a new phase. An increase in the concentration of impurities at individual points in the transition region of the composite may be due to interaction with silicon carbon at the

Table 5. Elemental composition of the composite at the points *1*–*5*, marked in Fig. 4.

Registered elements	Elemental composition of the composite, mass.%				
	1	*2*	*3*	*4*	*5*
Fe	–	–	0.20	–	0.08
Al	–	–	0.08	0.14	0.12
Ca	–	–	0.05	28.36	9.01
O	–	0.32	2.70	26.89	31.44
Si	–	46.06	25.71	5.52	6.53
C	100	53.62	71.26	39.09	52.82

infiltration front, resulting in the enrichment of the melt with impurities. Gradually, the delivery of the silicon melt through the pore structure to the infiltration front stops due to the filling of the pores with silicon carbide. As a result, the solid-phase interaction of silicon with carbon is completed at the infiltration front. Then the Al, Fe and Ca impurities in the melt begin to interact with carbon and can form the corresponding carbides on the surface of the pores. The high oxygen content at points *4* and *5*, marked in Fig. 4, may be due to the interaction of the chemically active phase with water (during processing of the workpiece with a diamond tool) and the formation, as noted in [17], hydroxides, for example, according to the reaction $Ca_2+8H_2O \rightarrow Ca(OH)_2+2CH_4$; $Ca(OH)_2+CO_2 = CaCO_3+H_2O$.

Conclusions

As a result of reactive infiltration of the silicon melt, porous carbon matrices, the apparent density of which $\rho_0 \leq 1.42\,g/cm^3$, turned out to be siliconized over the entire height of the workpiece, equal to 105 mm. An increase ρ_0 of the porous carbon matrix limits the height of infiltration of the silicon melt.

n carbon matrices, the apparent density of which is $\rho_0 \geq 1.452\,g/cm^3$, a transition region is observed between the siliconized and non-siliconized parts of the workpiece. The width of such a transition region decreases with increasing ρ_0 of the carbon matrix.

In the transition region, only SiC and graphite phases are present; the silicon melt entering this region completely enters into solid-phase interaction with carbon. The surface of the largest pores turned out to be covered with a layer of silicon carbide.

Reactive infiltration of molten silicon in a porous carbon matrix develops initially by wetting the surface (surface of diffusion) and forming a layer of silicon carbide. Further infiltration of the melt develops along the layer formed along silicon carbide under the action of capillary forces.

Funding

The work was carried out with financial support from the grant „of Foundation for Advanced Scientific Research“ No 2023/10 of Chelyabinsk State University.

Conflict of interest

The authors declare that they have no conflict of interest.

References

[1] M. Caccia, J. Narciso. Materials, **12** (15), 2425 (2019). DOI: 10.3390/mar12152425
[2] Y. Tong, S. Bai, X. Liang, Q.H. Qin, J. Zhai. Ceram. Intern., **42** (15), 17174 (2016). DOI: 10.1016/j.ceramint.2016.08.007
[3] S.L. Shikunov, V.N. Kurlov. ZhTF, **87** (12), 1871 (2017). (in Russian). DOI: 10.21883/JTF.2017.12.45212.2291
[4] M. Naikade, C. Hain, K. Kastelik, R. Brönnimann, G. Bianchi, A. Ortona, T. Graule, L. Weber. J. Eur. Ceram. Soc., **42** (5), 1984 (2022). DOI: 10.1016/j.jeurceramsoc.2022.01.004
[5] J. Roger, G. Chollon. Ceram. Intern., **45** (7), 8690 (2019). DOI: 10.1016/j.ceramint.2019.01.191
[6] O.Yu. Sorokin, I.A. Bubnenkov, Yu.I. Koshelev, T.V. Orekhov. Izv. vuzov, Khimiya i khim. tekhnologiya, **55** (6) 12 (2012) (in Russian).
[7] R. Israel, R. Voytovych, P. Protsenko, B. Drevet, D. Camel, N. Eustathopoulos. J. Mater. Sci., **45**, 2210 (2010). DOI: 10.1007/s10853-009-3889-6
[8] J.F. White, K. Forwald, L. Ma, D. Sichen. Metal. Mater. Trans. B, 45, 150 (2014). DOI: 10.1007/s11663-013-9947-0
[9] O. Dezellus, S. Jacques, F. Hodaj, N. Eustathopoulos. J. Mater. Sci., **40**, 2307 (2005). DOI: 10.1007/s10853-005-1950-7
[10] S. Kumar, A. Kumar, R. Devi, A. Shukla, A.K. Gupta. J. Europ. Ceram. Society, **29** (12), 2651 (2009). DOI: 10.1016/j.jeurceramsoc.2009.03.006
[11] J.C. Margiotta, D. Zhang, D.C. Nagle, C.E. Feeser. J. Mater. Res., **23** (5), 1237 (2008). DOI: 10.1557/JMR.2008.0167
[12] P. Sangsuwan, S.N. Tewari, J.E. Gatica, M. Singh, R. Dickerson. Metal. Mater. Trans. B, **30**, 933 (1999). DOI: 10.1007/s11663-999-0099-1
[13] A. Favre, H. Fuzellier, J. Suptil. Ceram. Intern., **29** (3), 235 (2003). DOI: 10.1016/S0272-8842(02)00110-4
[14] Y. Wang, S. Tan, D. Jiang. Carbon, **42** (8–9), 1833 (2004). DOI: 10.1016/j.carbon.2004.03.018
[15] P.J. Hofbauer, E. Rädlein, F. Raether. Adv. Eng. Mater., **21** (8), 1900184 (2019). DOI: 10.1002/adem.201900184
[16] V.A. Tyumentsev, A.G. Fazlitdinova. Izv. vuzov, Khimiya i khim. tekhnologiya, **65** (3) 6 (2022) (in Russian). DOI: 10.6060/ivkkt.20226503.6468
[17] V.A. Tyumentsev, S.I. Saunina, A.A. Sviridov, S.A. Podkopaev, N.P. Nonishneva. Journal of Inorganic Chemistry, **49**(5), 825 (2004).

Translated by V.Prokhorov